Revisiting and Redesigning Light-Activated Cyclic-Mononucleotide Phosphodiesterases

Robert Stabel [1], Birthe Stüven [1,2], Jan Niklas Hansen [2], Heinz G. Körschen [3], Dagmar Wachten [2,3] and Andreas Möglich [1,4,5,6]

*1 - **Lehrstuhl für Biochemie,** Universität Bayreuth, 95447 Bayreuth, Germany*
*2 - **Institute of Innate Immunity,** Universität Bonn, 53127 Bonn, Germany*
*3 - **Center of Advanced European Studies and Research (caesar),** 53175 Bonn, Germany*
*4 - **Research Center for Bio-Macromolecules,** Universität Bayreuth, Bayreuth, Germany*
*5 - **Bayreuth Center for Biochemistry & Molecular Biology,** Universität Bayreuth, 95447 Bayreuth, Germany*
*6 - **North-Bavarian NMR Center,** Universität Bayreuth, 95447 Bayreuth, Germany*

***Correspondence to Andreas Möglich:** Lehrstuhl für Biochemie, Universität Bayreuth, 95447 Bayreuth, Germany.*
andreas.moeglich@uni-bayreuth.de.
https://doi.org/10.1016/j.jmb.2019.07.011

Abstract

As diffusible second messengers, cyclic nucleoside monophosphates (cNMPs) relay and amplify molecular signals in myriad cellular pathways. The triggering of downstream physiological responses often requires defined cNMP gradients in time and space, generated through the concerted action of nucleotidyl cyclases and phosphodiesterases (PDEs). In an approach denoted optogenetics, sensory photoreceptors serve as genetically encoded, light-responsive actuators to enable the noninvasive, reversible, and spatiotemporally precise control of manifold cellular processes, including cNMP metabolism. Although nature provides efficient photoactivated nucleotidyl cyclases, light-responsive PDEs are scarce. Through modular recombination of a bacteriophytochrome photosensor and the effector of human PDE2A, we previously generated the light-activated, cNMP-specific PDE LAPD. By pursuing parallel design strategies, we here report a suite of derivative PDEs with enhanced amplitude and reversibility of photoactivation. Opposite to LAPD, far-red light completely reverts prior activation by red light in several PDEs. These improved PDEs thus complement photoactivated nucleotidyl cyclases and extend the sensitivity of optogenetics to red and far-red light. More generally, our study informs future efforts directed at designing bacteriophytochrome photoreceptors.

Introduction

Various cellular pathways in both prokaryotes and eukaryotes harness diffusible second messengers to amplify and relay molecular signals in time and space [1]. Cyclic nucleotides represent a widespread class of second messengers that underpin a cohort of physiological responses. In eukaryotes, the two predominant cyclic mononucleotides, 3′, 5′-cyclic adenosine and guanosine monophosphate (cAMP and cGMP) [2–4], bind to the protein kinases A and G [5,6], cyclic nucleotide-gated (CNG) ion channels [7], Epac (exchange protein directly activated by cAMP) [8] and popeye-domain-containing proteins [9], and thereby allosterically regulate the activity of these entities. With but few exceptions [10,11], prokaryotes lack cGMP signaling but widely employ cAMP to regulate gene expression, prominently so in the context of catabolite repression [12,13]. The cyclic nucleoside monophosphates (cNMPs) cAMP and cGMP are generally produced by nucleotidyl cyclases from adenosine and guanosine triphosphate (ATP and GTP). Phosphodiesterases (PDE) mediate the hydrolytic breakdown of cNMPs to the (non-cyclic) 5′-adenosine and 5′-guanosine monophosphates (AMP and GMP), respectively. Mammals possess 11 different PDE families, which subdivide into several isoforms [15,16]. Depending

on family, these PDEs are specific for either cAMP, cGMP or both. Although the precise protein architecture differs between families, the mammalian PDEs generally comprise N-terminal domains that process signal input and C-terminal catalytically active effector domains. As a case in point, the cAMP/cGMP-specific PDE2A adopts a homodimeric structure, in which two regulatory GAF domains (denoted GAF-A and GAF-B), connect to the C-terminal PDE domain via a parallel α-helical coiled-coil linker [17] (Fig. S1a). cGMP binding to GAF-B prompts an about 4-fold increase in catalytic turnover by displacing an autoinhibitory protein loop (termed H loop) from the PDE active site [17].

Inside the cell, the activities of nucleotidyl cyclases and PDEs are tightly orchestrated to allow generation of complex spatiotemporal cNMP gradients that underpin downstream physiological responses. Implements that modulate the intracellular amounts of cNMPs with precision in space and time are hence particularly applicable for probing and elucidating pertinent signal processes. Optogenetics [18], referring to the monitoring and control by light of cellular events via genetically encoded agents, has contributed versatile tools for the study of cNMP signal transduction [19,20]. In specific, certain sensory photoreceptors occurring in nature act as photoactivated adenylyl cyclases (PAC) and ramp up cAMP production upon light application [21–26]. While most of these cyclases respond to blue light, a group of PACs sensitive to red/far-red light were engineered by recombining cyclase effector modules with the so-called photosensory core modules (PCMs) of bacterial phytochrome (BphP) receptors [27–30]. The phytochrome PCM comprises tandem PAS, GAF, and PHY domains and harbors a linear tetrapyrrole (bilin) chromophore, biliverdin (BV) in case of BphPs [31]. In darkness, conventional BphPs assume the red-light-absorbing Pr state with their BV cofactor in its 15*Z* conformation. Red light drives the photoisomerization of BV to the 15*E* state, giving rise to the far-red-light-absorbing Pfr form; the reversion to the Pr state occurs in a slow thermal reaction or can be actively driven by far-red light. By contrast, in bathyphytochromes, the Pfr state is the thermodynamically stable state assumed in darkness [31]. Structures of the isolated PCM of the conventional BphP from *Deinococcus radiodurans* (*Dr*BphP) revealed that the chromophore isomerization induces refolding of a protrusion of the PHY domain, denoted tongue, from a β-sheet conformation in Pr to an α-helical conformation in Pfr, which in turn promotes quaternary structural rearrangements in the dimeric receptor [32,33]. BphP-based actuators are attractive as optogenetic tools for at least three principal reasons: first, long-wavelength light penetrates biological tissue more deeply than light of shorter wavelengths [34]; second, BphPs can be bimodally switched by red and far-red light, thus affording enhanced spatiotemporal resolution in optogenetics [35]; and third, BV widely occurs in mammalian tissue as a heme degradation product, thus obviating exogenous chromophore addition and greatly facilitating optogenetic applications [27,36,37]. In addition to PACs, a number of photoactivated guanylyl cyclases are available in nature or by protein engineering [24,38–42]. By contrast, there has been a relative dearth of light-regulated actuators that would mediate the hydrolytic breakdown of cNMPs. To fill this gap, we previously constructed the light-activated PDE LAPD via recombination of the *Dr*BphP PCM and the effector module of *Homo sapiens* PDE2A (*Hs*PDE2A) [36] (Fig. 1a). Similar to the parental *Hs*PDE2A, LAPD hydrolyzed both cAMP and cGMP with comparable rates and affinities; red light elevated the maximum catalytic turnover of LAPD by around 6-fold. However, although far-red light partially reverted this increase in turnover, the reaction was incomplete, hinting at inefficient Pfr → Pr photoconversion [36]. Since, a PDE covalently linked to a microbial rhodopsin photosensor unit has been discovered in the choanoflagellate *Salpingoeca rosetta* [43,44]. Biochemical analyses revealed a preference for cGMP over cAMP, and an around 7-fold increase in cGMP affinity upon light absorption [45].

Against this backdrop, we here report the engineering of cNMP-specific PDEs that respond to red/far-red light and improve on LAPD regarding extent and reversibility of switching. The analysis of multiple PDE variants identifies sequence motifs underpinning efficient regulation by light and thus establishes refined design rules for constructing light-activated PDEs. As we showcase for the gating of CNG channels in mammalian cells, the novel LAPD variants can be deployed to probe and control cNMP-associated cellular processes. Light-regulated PDEs thus complement the diverse set of PACs and enrich the arsenal of optogenetics [19,46].

Results

Modular construction of cyclic-mononucleotide Phosphodiesterases

To engineer derivative red-/far-red-light-responsive PDEs, we revisited the original LAPD design, which was informed by the structural homology between the sensor modules of BphPs and certain mammalian PDEs [36]. Despite vastly different phylogenetic origin, both entities share a parallel homodimeric architecture, structurally homologous N-terminal sensor domains and central α-

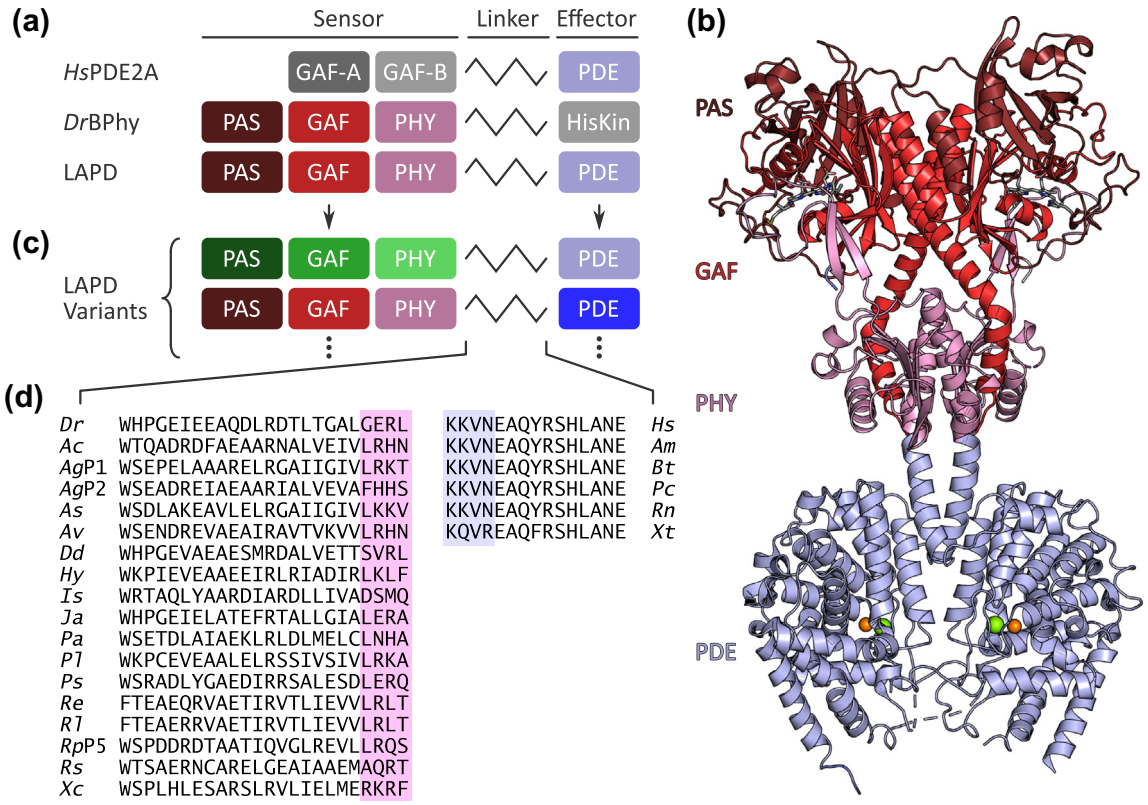

Fig. 1. Engineering of light-regulated cNMP-specific PDEs. (a) The prototype LAPD originated from the modular recombination of the *Deinococcus radiodurans* bacteriophytochrome (*Dr*BphP) photosensor, comprising PAS-GAF-PHY domains, and the *Homo sapiens* PDE2A (*Hs*PDE2A) effector domain [36]. (b) Structural model of LAPD based on the structures of the engineered BphP PagC (PDB code 6FHT) [28] and *Hs*PDE2A (3IBJ) [17]. The PAS, GAF, PHY and PDE domains are colored in dark red, red, pink and light blue, respectively; the green and orange spheres in the PDE domain denote magnesium and zinc ions. (c) To generate derivative light-regulated PDEs, the photosensor and/or the effector moieties of LAPD were exchanged for modules from homologous BphPs and PDEs. (d) Partial sequence alignment of the linker region of BphPs and PDEs used in the construction of LAPD derivatives. The top line denotes the fusion between *Dr*BphP and *Hs*PDE2A and corresponds to the prototypical LAPD. Residues near the fusion site are highlighted by pink and blue shading. Species abbreviations for the BphP PCMs are *Ag*P1, *Agrobacterium tumefaciens* BphP P1; *Ag*P2, *A. tumefaciens* BphP P2; *Ac*, *Azorhizobium caulinodans*; *As*, *Acaryochloris* sp. CCMEE 5410; Av, *Agrobacterium vitis*; *Dd*, *Deinococcus deserti*; *Dr*, *Deinococcus radiodurans*; *Hy*, *Hymenobacter swuensis*; *Is*, *Idiomarina* sp. A28L; *Ja*, *Janthinobacterium* sp. CG23_2; *Pa*, *Pseudomonas aeruginosa*; *Pl*, *Pleurocapsa* sp. PCC7319; *Ps*, *Pseudomonas syringae*; *Re*, *Rhizobium etli*; *Rl*, *Rhizobium leguminosarum*; *Rp*P5, *Rhodopseudomonas palustris* BphP P5; *Rs*, *Rhodobacter sphaeroides*; and *Xc*, *Xanthomonas campestris*. PDE modules derive from *Am*, *Alligator mississippiensis*; *Bt*, *Bos taurus*; *Hs*, *Homo sapiens*; *Pc*, *Phascolarctos cinereus*; *Rn*, *Rattus norvegicus*; and *Xt*, *Xenopus tropicalis*.

helical spines, which coincide with the C_2-symmetry axes and feed into coiled-coil linkers connecting to the respective effector modules (Fig. S1). At the time, structural information on the complete *D. radiodurans* PCM was lacking, and the LAPD design relied on the PCM structure of *Pseudomonas aeruginosa* BphP (*Pa*BphP) in its Pfr state [47]. Although eventually fruitful, this design blueprint suffered from several shortcomings: first, in the actual LAPD, the *Hs*PDE2A effector is fused to the *Dr*BphP PCM, rather than to the *Pa*BphP PCM (Fig. 1a); second, unlike *Dr*BphP, *Pa*BphP is a bathyphytochrome; third, the coiled-coil linker was not resolved in the *Pa*BphP structure, thus leaving ambiguous the precise molecular arrangement of this structural region in LAPD. Arguably due to these deficits, the design initially favored a chimeric receptor, denoted LAPD+2, with two additional residues in the coiled-coil linker relative to LAPD, but devoid of light-regulated PDE activity [36]; subsequent removal of these two residues gave rise to the light-responsive LAPD. Structures of the complete PCM of *Dr*BphP in both the Pr and Pfr states have since become available [32,33], as has that of the engineered BphP-guanylyl cyclase PagC, which atomically resolves the coiled-coil linker of *Dr*BphP [28]. Informed by these data, we updated our structural model for LAPD (Figs. 1b and S1). Whereas the original model placed the BphP PCM and the PDE effector of one chain on opposite sides

of the α-helical spine traversing the homodimeric receptor, the new model positions them on the same side. Moreover, the revised model enables structural modeling of the fusion site in LAPD with enhanced confidence, see below.

We hypothesized that the limited reversibility of light-dependent activation evidenced in LAPD might be rooted in the *Dr*BphP PCM. This view is borne out in a recently engineered PAC that shares with LAPD the *Dr*BphP PCM and likewise exhibits limited photo reversibility upon prior activation by light [28,29]. By contrast, replacing the PCM of *Dr*BphP with that of *Deinococcus deserti* BphP (*Dd*BphP) yielded a PAC with photoreversible adenylyl cyclase activity [29]. We hence generated LAPD variants by substituting the PCM of *Dr*BphP for those of 17 different BphPs (Fig. 1c), some of which were previously described as conventional and bathyphytochromes, respectively [48]. In choosing so, we sought to cover a wide range of BphP modules with different properties, and to thereby increase the chance of eventually obtaining enhanced LAPD variants. For the facile assessment of PDE activity and response to light, we resorted to an enzymatic assay that can be conducted in crude cell lysate [49]. Briefly, the hydrolysis of cNMP to NMP is accompanied by proton release, thus leading to acidification of weakly buffered solutions, which is readily detectable with the pH-sensitive fluorescein derivative BCECF [50] (Fig. 2a). We thus expressed LAPD in *Escherichia coli* along with *Synechocystis* sp. heme oxygenase 1 (*Ss*HO) [51], that supplies biliverdin, and ascertained production of the holo enzyme by green coloration of the bacterial suspension and zinc-induced fluorescence of the bilin chromophore [52]. Following cell lysis, PDE activity can be directly probed in bacterial lysate. Within this assay, LAPD showed an initial drop in normalized BCECF fluorescence of -3.9×10^{-3} min^{-1} when incubated with saturating amounts of 2 mM cGMP in darkness and of -1.9×10^{-2} min^{-1} when illuminated with 670-nm light. In the following, we report results from this lysate assay as unitless BCECF activity values normalized to the signal of LAPD under red light (arbitrarily set to 1.0). Previous studies on LAPD and related homodimeric receptors had pinpointed the length and, to lesser extent, the sequence of coiled-coil linkers between sensor and effector modules as crucial for overall activity and responsiveness to light [27,28,36,53,54]; even the mere insertion or omission of single residues within this region can utterly alter light-dependent receptor output. When constructing fusions between the various BphP PCMs and the *Hs*PDE2A effector module, we thus retained the same linker register as in LAPD (Fig. 1d). We first ascertained expression in *E. coli* by green coloration and Western blot (Fig. S2), which revealed that almost all BphP-PDE variants were expressed to similar extent as LAPD. Merely, the variant based on

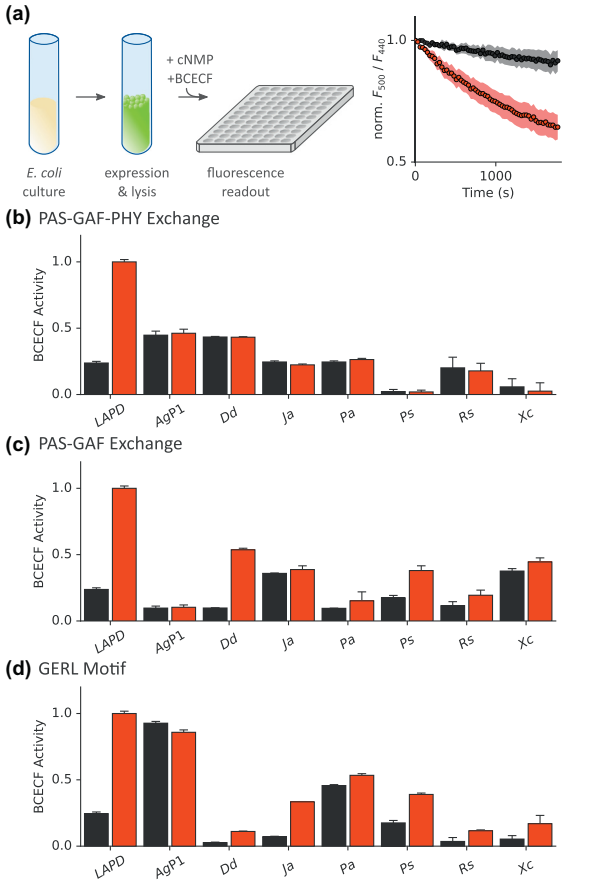

Fig. 2. Screening for light-regulated cNMP-specific PDE variants. (a) Candidate PDEs are expressed in *E. coli* and assessed for light-regulated activity in bacterial lysate. As cNMP hydrolysis entails proton release, the progressive acidification of a weakly buffered solution can be monitored over time via the pH-sensitive fluorophore BCECF [49]. As exemplarily shown for LAPD, the assay provides a facile readout for candidate PDEs in their dark-adapted states (black) and following red-light exposure (red). In panels b through d, the apparent cGMP hydrolysis activities of candidate PDEs are reported as the initial slopes in the BCECF assays, normalized to the signal obtained for LAPD upon red-light stimulation. All data represent mean ± s.d. of four biological replicates. (b) The PAS-GAF-PHY photosensor of LAPD was exchanged for the corresponding modules from homologous bacteriophytochromes (BphP) and cGMP hydrolysis of the resultant PDE variants was measured. Species abbreviations are provided in Fig. 1. (c) The PAS and GAF domains of LAPD were substituted for the corresponding domains of other BphPs (see Fig. S4). (d) The linker regions of select BphP-PDE variants from panel b were modified to resemble the GERL motif found in the light-responsive LAPD prototype (see Figs. 1d and S5). In case of *Rs*-*Hs*PDE2A and *Xc*-*Hs*PDE2A variants, data for the most strongly light-regulated variants with the linker sequences GERT and GERF are shown.

the PCM from *Rhodopseudomonas palustris* BphP P5 exhibited attenuated yet detectable expression. We then assessed the cGMP hydrolysis activity of these variants in bacterial lysate by BCECF fluorescence (Figs. 2b and S3a). All tested BphP-PDE variants exhibited lower PDE activity compared to LAPD, but none showed significant red-light dependence of activity. Likewise, illumination with far-red light did not elicit any activity increase. While the differences in the observable overall activity might be attributable to variations in functional expression and specific activity, we were puzzled by the complete lack of light responsiveness. Evidently, the design template underpinning LAPD is not directly transferrable to homologous BphP PCMs, at least not without further optimization.

Imparting light sensitivity on cyclic-mononucleotide Phosphodiesterases

We tentatively ascribed the consistent lack of light responsiveness in the LAPD variants to deficient allosteric coupling between the bacterial PCM and the eukaryotic PDE module. To enhance this coupling and thus attain light-regulated PDE activity, we pursued two concurrent strategies. In a first approach, we replaced the PAS and GAF domains of the light-responsive LAPD for those of homologous BphPs while retaining the *Dr*PHY and *Hs*PDE2A domains. Although this replacement generates an additional seam between the GAF and PHY domains deriving from different BphPs, it preserves the critical junction between the PHY and PDE domains of LAPD. We selected 10 of the above BphPs and created chimera between their PAS-GAF portions and the PHY-PDE fragment of LAPD (Fig. S4). As before, we coexpressed the resultant BphP-PDE variants with *Ss*HO (Fig. S2) and assessed their cGMP hydrolytic activity in darkness and under 670-nm light by BCECF fluorescence (Figs. 2c and S3b). Out of the 10 variants, 7 showed constitutive hydrolysis activity, but 3 variants, harboring the PAS-GAF fragments of *Dd*BphP, *Pseudomonas syringae* BphP (*Ps*BphP) and *Agrobacterium tumefaciens* P2 (*Ag*P2), significantly increased activity in response to red light relative to darkness. In particular, the variants based on *Dd*BphP and *Ps*BphP, referred to as *DdDr-Hs*PDE2A and *PsDr-Hs*PDE2A, exhibited red-light-induced increases in BCECF activity of around 5.5-fold and 2.2-fold, respectively.

In light of these findings, we reasoned that the configuration of the linker around the junction between the PHY and PDE domains of LAPD might be particularly relevant for efficient coupling between photosensor and effector. Based on amino acid sequence and full-length structures of BphP receptors [28,56–58], the linker of LAPD is expected to adopt a continuous α helix, with the BphP PCM terminating in the four residues Gly-503, Glu-504, Arg-505 and Leu-506 (GERL in single-letter code), and the PDE effector continuing with the residues Lys-507 and Lys-508 (KK). As illustrated by the LAPD homology model (Figs. 1b and 3a), residues E504 and K508 are appropriately spaced to potentially form an *i*, *i* + 4 salt bridge that traverses the seam between the PCM and PDE moieties. In the vicinity, two additional salt bridges are formed between R505 and E426 within the PHY domain, and between K507 and E511 within the PDE part. To probe the relevance of this region of LAPD, we exchanged individual residues of the GERL motif for amino acids found in the corresponding position of the homologous BphPs (Figs. 1d and 3b–e). In summary, almost all substitutions within the GERL motif severely attenuated the light response or entirely abolished it. As exceptions, the exchanges of E504 to alanine or arginine preserved light responsiveness to significant extent, as did the replacement of L506 for isoleucine. To further probe the functional role of the potential E504:K508 and K507:E511 salt bridges running along the linker helix, we also substituted the two lysine residues (Fig. 3f). Replacement of K507 for serine, the corresponding amino acid present in *Dr*BphP [36] (see Fig. S4), resulted in a PDE variant with constitutively low activity and minute light response. By contrast, the exchange of K508 to alanine neither affected PDE activity nor light regulation. Although it is challenging to fully rationalize the various substitutions at a structural and functional level, several general aspects emerge. First, the linker segment of LAPD is highly sensitive to structural perturbations, with most residue exchanges, even those of conservative type, impairing overall activity and light responsiveness. Second, a putative salt bridge between E504 and K508, if present at all in LAPD, is not essential for productive signal transduction. Third, although we probed more than 20 sequence variations of the linker region, the original motif proved the best-suited for robust activity and regulation by light.

Given the pronounced preference for the ^{503}GERL^{506} sequence at the BphP-PDE junction in LAPD, we investigated whether light sensitivity can be bestowed on the above light-inert BphP-PDE receptors via introduction of said sequence. To this end, we selected seven variants, consisting of the intact PCMs (PAS-GAF-PHY) of homologous BphPs and the *Hs*PDE2A effector module (see Fig. 2b), and stepwise altered their linker segments toward the GERL motif by exchanging between two and four residues (Figs. 2d, S2 and S5). BCECF activity measurements revealed that this approach indeed succeeded in converting five out of the seven BphP-PDEs into light-activated receptors. Although these light-regulated variants generally showed BCECF activity lower than LAPD, they exhibited similar factors of activation upon red-light exposure.

Notably, in certain of these variants, light responsiveness was only achieved when retaining the terminal residue of the original PCM rather than altering it to leucine. For example, in the *Rs-Hs*PDE2A receptor, comprising the PCM of *Rhodobacter sphaeroides* BphP, red light prompted an activity increase when the corresponding residue was the original threonine (GER**T**) but not when it was leucine. Perplexingly, in LAPD the replacement of leucine in this position for threonine abrogated light responsiveness (see Fig. 3).

Modular exchange of Phosphodiesterase effector modules

The above experiments compellingly illustrate that the engineering of derivative red-light-regulated PDEs via modification of the BphP photosensor module is challenging. In a parallel approach, we substituted the effector unit of LAPD for the catalytic domains from five vertebrate PDE2A enzymes (Fig. 1d), an approach that benefits from high levels of sequence homology between 81% and 98%. With the original LAPD as template, we constructed fusions between the *Dr*BphP PCM and the homologous PDE2A effectors, expressed the resultant receptors (Fig. S2) and assessed cGMP hydrolysis in bacterial lysate (Fig. S6). Whereas two of these receptors showed low activity and no significant response to illumination, the variants *Dr-Bt*PDE2A, *Dr-Pc*PDE2A, and *Dr-Xt*PDE2A, based on the PDE2A enzymes from *Bos taurus*, *Phascolarctos cinereus* and *Xenopus tropicalis*, respectively, exhibited light-stimulated activity. Notably, the *Dr-Bt*PDE2A receptor displayed reduced activity in darkness relative to LAPD, but increased activity upon red-light exposure, translating into a much more pronounced regulation by light. Compared to the above efforts at derivatizing LAPD that centered on the BphP photosensor module, the exchange of the effector module proved strikingly more successful and yielded PDE variants with stringent light regulation.

To better characterize cNMP hydrolysis and response to light, we expressed and purified *Dr-Bt*PDE2A, *Dr-Pc*PDE2A, and *Dr-Xt*PDE2A, as well as the above variants *Dd*GERL-*Hs*PDE2A and *DdDr-Hs*PDE2A (see Fig. 2c, d). UV/vis spectroscopy indicated that in darkness, all these BphP-PDEs predominantly assume their Pr state, which maximally absorbs around 700 nm (Fig. 4). In case of *DdDr-Hs*PDE2A, partial population of the Pfr state, maximally absorbing around 750 nm, was evident even in darkness. Red light (670 nm) drove the Pr → Pfr transition in the PDE variants to similar but slightly lower extent relative to LAPD. As an exception, the degree of Pr → Pfr photoconversion in *DdDr-Hs*PDE2A was markedly reduced, and both the Soret and the Q bands, at around 400 and 700 nm, respectively, exhibited shoulders. These observations point toward impaired photochemistry, which presumably results from the recombination of the PAS-GAF domains from one BphP with the PHY domain from another in this variant. Subsequent illumination with far-red light (780 nm) reverted the spectra to their dark-adapted states in all cases.

We went on and quantified cGMP hydrolysis at 1 mM substrate concentration by the BphP-PDE variants in darkness and following red-light application via high-performance liquid chromatography

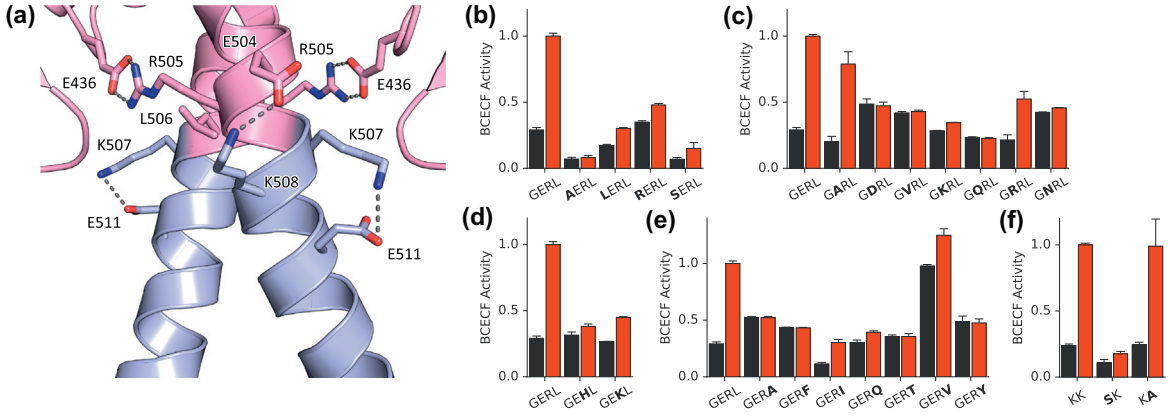

Fig. 3. Probing the linker region in LAPD. (a) Close-up of the linker region in the LAPD structural model (see Fig. 1b). Residues around the seam between photosensor and effector are shown in stick representation. Salt bridges observed in the structures of PagC [28] and *Hs*PDE2A [17] or inferred from the model are indicated. (b–e) Individual residues within the ^{503}GERL^{506} motif of LAPD at the C-terminal end of the photosensor unit were exchanged for residues observed at the corresponding position in the homologous bacteriophytochromes (see Fig. 1d). Activity of the resultant LAPD variants in their dark-adapted states (dark) or upon red-light exposure (red) was assessed by BCECF fluorescence. All data represent mean ± s.d. of four biological replicates. (f) Exchanges of the residues K507 and K508 within the PDE fragment of the linker region.

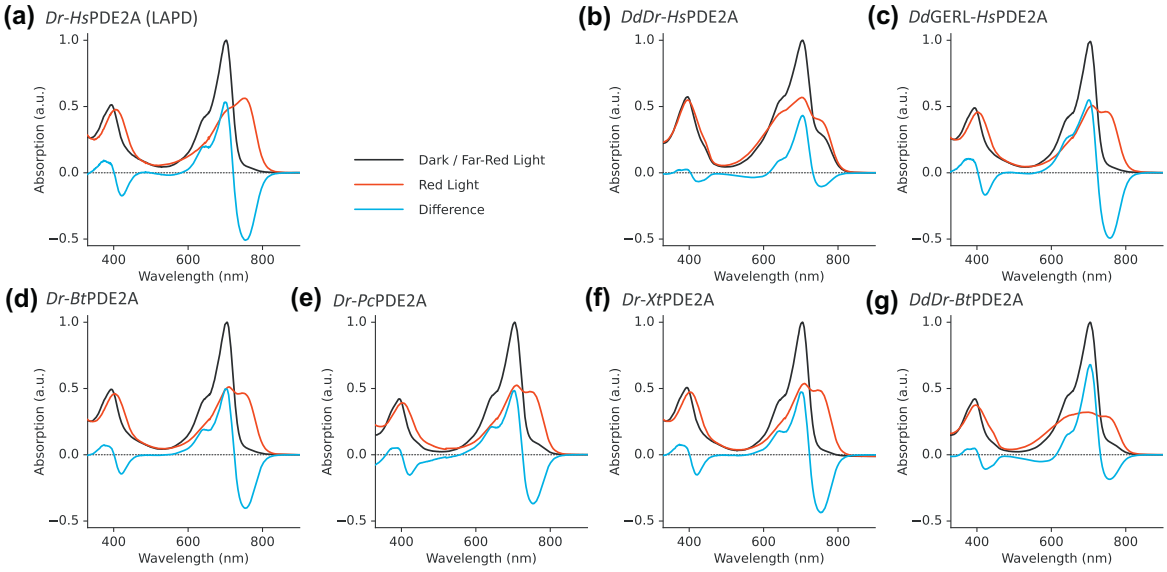

Fig. 4. UV/vis-absorption spectra of BphP-PDE variants in their dark-adapted states (black) and after red-light exposure (red). The cyan curves show dark–light difference spectra. Spectra were normalized to the peak maximum of the Q band in the dark-adapted state. (a) LAPD. (b) *DdDr-Hs*PDE2A. (c) *Dd*GERL-*Hs*PDE2A. (d) *Dr-Bt*PDE2A. (e) *Dr-Pc*PDE2A. (f) *Dr-Xt*PDE2A. (g) *DdDr-Bt*PDE2A.

(Fig. 5). At 29 °C, LAPD displayed specific cGMP hydrolysis activities of (2.0 ± 0.1) µmol (nmol enzyme min)$^{-1}$ in darkness and (11.0 ± 0.3) µmol (nmol enzyme min)$^{-1}$ under red light, similar to our previous findings [36]. Compared to LAPD, most variants had lower specific activities in both darkness and red light, and somewhat reduced degrees of light stimulation between 2.9-fold and 5.5-fold. However, *Dr-Bt*PDE2A exhibited higher activation of around 8.0-fold and maximal specific activity of (13.5 ± 0.1) µmol (nmol enzyme min)$^{-1}$ under red light. We next probed the reversibility of activation in the BphP-PDEs by exposing them successively to red and far-red light, followed by enzymatic assays. As observed previously [36], LAPD could not be fully switched off by far-red light and hydrolyzed cGMP with a turnover of (4.3 ± 0.1) µmol (nmol enzyme min)$^{-1}$. Notably, the above spectroscopic measurements used the same illumination protocol and showed that LAPD fully assumes the Pr configuration of its chromophore under these conditions, pointing to at least partial uncoupling of photochemical events and catalytic activity. Although two BphP-PDE variants, *Dr-Pc*PDE2A and *Dd*GERL-*Hs*PDE2A, shared with LAPD an incomplete or even absent reversal of hydrolysis activity under far-red light, the other variants showed markedly enhanced properties. In *Dr-Bt*PDE2A, far-red light returned hydrolysis activity to (2.3 ± 0.1) µmol (nmol enzyme min)$^{-1}$, almost the same value as in darkness. In the remaining variants, *Dr-Xt*PDE2A and *DdDr-Hs*PDE2A, far-red light completely reverted prior activation by red light. Thus, the extent of far-red-light-driven activity reversal in (engineered) bacteriophytochromes is apparently determined by both the photosensor and effector modules: whereas the *Dr*BphP PCM supported complete reversal when connected to *Xt*PDE2A, it failed to do so in the context of other effectors [29,36]. We also assessed cAMP hydrolysis in the PDE variants and found overall similar specific activities and degrees of light activation (Figs. S7 and 5i). As an exception, the specific cAMP hydrolysis activity of LAPD under red light amounted to (5.7 ± 0.1) µmol (nmol enzyme min)$^{-1}$, somewhat lower than observed for cGMP hydrolysis but consistent with our previous measurements [36]. By recombining the chimeric *DdDr*-PCM and the *Bt*PDE, we also produced the variant *DdDr-Bt*PDE2A, which, however, did not lead to an improvement of catalytic properties over *DdDr-Hs*PDE2A. As optogenetic actuators are often deployed in living animals, we also determined the cGMP and cAMP hydrolysis activities of LAPD and *Dr-Bt*PDE2A at 37 °C (Fig. S8). At this temperature, the cGMP and cAMP hydrolysis activities under red light were around 40% higher than at 29 °C. Interestingly, the activities of LAPD in darkness or under far-red light were slightly reduced at the higher temperature, thus improving its regulatory efficiency.

Optogenetic application of light-regulated Phosphodiesterases in mammalian cells

Having engineered a set of red-light-responsive BphP-PDEs, we next addressed whether they allow to regulate signaling in mammalian cells. We transfected HEK-TM cells, stably expressing a

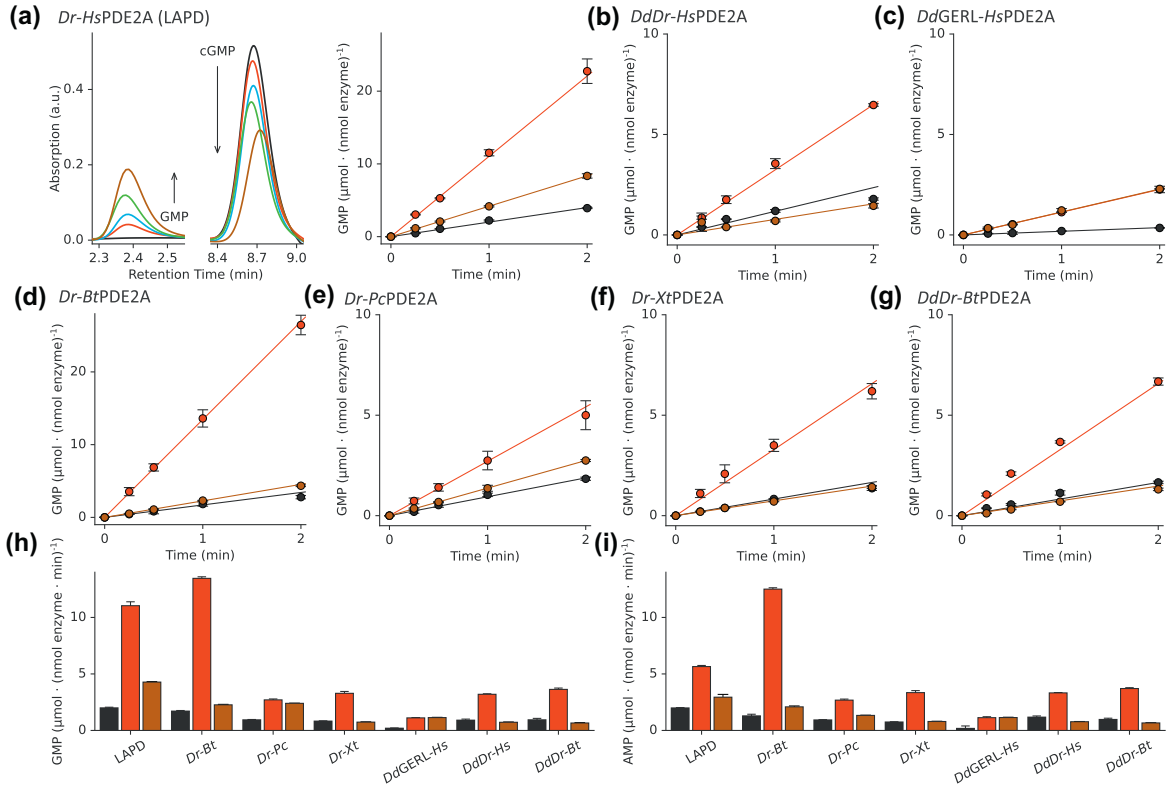

Fig. 5. Analysis by high-performance liquid chromatography of cNMP hydrolysis in light-regulated PDE variants. (a) (Left) As exemplarily shown for a hydrolysis reaction catalyzed by red-light-exposed LAPD, the amount of substrate cGMP decreases over time and that of the product GMP increases over time. (reaction times of 0, 0.25, 0.5, 1 and 2 min, as indicated by the arrows). (Right) Hydrolysis of 1 mM cGMP was assessed for dark-adapted (black) and for red-light-exposed LAPD (red; 670 nm), as well as for LAPD exposed first to red light and then to far-red light (brown; 780 nm). All data represent mean ± s.d. of three biological replicates. (b–g) cGMP hydrolysis data for the PDE variants *DdDr-Hs*PDE2A, *Dd*GERL-*Hs*PDE2A, *Dr-Bt*PDE2A, *Dr-Pc*PDE2A, *Dr-Xt*PDE2A and *DdDr-Bt*PDE2A. (h) Overview of cGMP turnover in the different PDE variants in their dark-adapted forms (black), following red-light illumination (red), and after successive exposure to red and far-red light (brown). (i) Overview of cAMP turnover in the different PDE variants (see Fig. S7).

variant of the cyclic nucleotide-gated ion channel CNGA2, denoted CNGA2-TM [59], with the genes for LAPD, *Dr-Bt*PDE2A, *Dr-Pc*PDE2A and *Dr-Xt*PDE2A. To readily monitor expression and facilitate the generation of stable cell lines, an mCherry tag was fused to the C terminus of these PDEs. Using antibiotics selection, we isolated cell clones that stably express the different BphP-PDEs and the CNG channel, as confirmed by fluorescence microscopy and Western blot (Fig. 6a, b). We then analyzed catalytic activity and response to illumination of these PDEs in the HEK-TM cells at 29 and 37 °C using a coupled reporter assay similar to our previous studies (Fig. 6c) [36]. To this end, the cells were loaded with a calcium (Ca^{2+})-sensitive fluorophore and treated with the water-soluble forskolin derivative NKH477 to stimulate endogenous adenylyl cyclase activity. The resultant increase in intracellular cAMP prompts opening of the CNG channel, prompting Ca^{2+} influx from the exterior and fluorescence increase. Upon reaching a steady-state, the PDEs were activated by red light, thus reducing intracellular cAMP and, in turn, attenuating Ca^{2+} influx and fluorescence. For normalization of the fluorescence signals, the Ca^{2+} ionophore ionomycin was added at the end of each experiment. In the non-transfected HEK-TM cells, NKH477 addition caused fluorescence to gradually increase to a plateau of around half-maximal normalized fluorescence (Figs. 6d and S9a). In the stable LAPD cell line, NKH477 also triggered a fluorescence increase to a constant, albeit lower level of around 0.13 (Fig. 6d). The lower fluorescence amplitude is likely due to basal PDE activity in darkness, consistent with the above BCECF and HPLC experiments and earlier measurements [36]. Illumination with red light resulted in a decrease of the fluorescence signal to baseline, indicative of light-activated PDE activity. Notably, in these experiments, no exogenous biliverdin was added, demonstrating that the endogenous supply

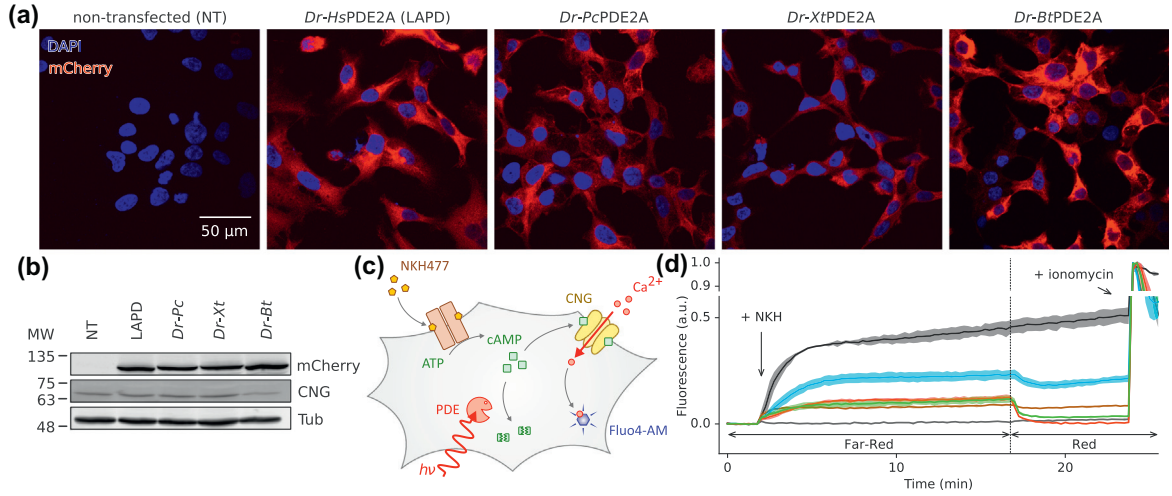

Fig. 6. Optogenetic control of cyclic adenosine monophosphate (cAMP) in mammalian cells. (a) HEK-TM cells, stably expressing a cyclic nucleotide-gated (CNG) ion channel, were stably transfected with mCherry-tagged LAPD, *Dr-Bt*PDE2A, *Dr-Pc*PDE2A or *Dr-Xt*PDE2A and observed by fluorescence microscopy. The elevated mCherry signal relative to a non-transfected control (NT) indicates PDE expression. (b) Cells from panel a were analyzed by Western blot, stained with antibodies directed against mCherry, the CNGA2 channel, and β tubulin. Sizes of a molecular weight (MW) marker are indicated in units of kDa. (c) Schematic of the coupled PDE reporter assay in the HEK-TM cells. Treatment with 100 µM NKH477 stimulates endogenous adenylyl cyclase activity and leads to a build-up of intracellular cAMP. In turn, the CNG channels open, thus resulting in Ca^{2+} influx and elevated fluorescence of the Ca^{2+}-sensitive dye Fluo4-AM. (d) Cell lines were initially incubated under far-red light at 37 °C, and NKH477 was added after 2 min. At 17 min, the cells were illuminated with red light (690 nm), and after another 6 min, the cell-permeabilizing ionophore ionomycin was added. Fluo4-AM fluorescence was monitored throughout the experiment and normalized to its maximum value reached after ionomycin addition. Lines and shaded areas represent mean normalized fluorescence ± s.d. of four biological replicates for the PDE lines and of two for the positive and negative controls. Non-transfected HEK-TM cells are shown in black, the LAPD cell line in red, *Dr-Bt*PDE2A in brown, *Dr-Pc*PDE2A in green and *Dr-Xt*PDE2A in blue; the bottom gray trace shows results from non-transfected HEK-TM cells that were not stimulated with NKH477.

suffices to evoke light responses, in line with previous observations [27,28,36]. We observed similar responses to NKH477 addition and illumination in the stable cell lines expressing *Dr-Pc*PDE2A and *Dr-Xt*PDE2A. For the latter, the fluorescence signal reached altogether higher levels in darkness, but the amplitude of reduction under red light was comparable (Fig. 6d). The on average higher fluorescence readings for *Dr-Xt*PDE2A may reflect different expression levels and a lower specific hydrolysis activity in this variant (see Fig. 5). By contrast, several stable *Dr-Bt*PDE2A cell lines that we tested all exhibited suppressed responses to NKH477 addition and were not stimulated by red-light exposure. As a possible reason, the expression levels and the specific activity of this PDE in the current cellular setting might have been too high, thus suspending significant cAMP accumulation upon NKH477 addition even under non-activating conditions. To test this hypothesis, we transiently transfected HEK-TM cells with *Dr-Bt*PDE2A, which leads to heterogenous and overall lower expression. As a corollary, NKH477 addition induced a stronger fluorescence increase in these cells than in the stable LAPD cell line; subsequent exposure to red light prompted a fluorescence decrease albeit of lower amplitude (Fig. S9b). These experiments demonstrate the principal functionality of *Dr-Bt*PDE2A in mammalian cells, but also indicate that, as for other optogenetic tools [35], the cellular expression level needs to be properly adjusted.

Discussion

Optogenetic control of cyclic mononucleotides

Through the recombination of bacteriophytochrome photosensor and vertebrate PDE effector modules, we engineered receptors that catalyze cAMP/cGMP hydrolysis and can be activated by red light. Compared to the LAPD blueprint [36], certain of the present BphP-PDE variants exhibit improved switching in that illumination with far-red light fully undoes prior activation with red light. Of particular note, the *Dr-Bt*PDE2A variant displays not only enhanced reversibility but also higher and more strongly light-regulated hydrolysis activity. Thus, this PDE variant represents an improvement over

LAPD and appears as a tool-of-choice for red-/far-red-light-regulated cNMP hydrolysis. As we demonstrate (see Fig. 6), LAPD, *Dr*-*Bt*PDE2A and several other PDE variants can be deployed optogenetically in mammalian cells to regulate by light cNMP-dependent physiological processes, for example, the ion flux through CNG channels. These studies also pinpoint a frequent challenge [20,35] associated with optogenetic applications: the desired light-induced physiological effects may only manifest to full extent (or even at all) if the cellular expression level and activity of the optogenetic actuator employed fall within appropriate intervals, and the ideal tool may hence depend on cellular context. For a given application scenario, these parameters may be demanding to gauge upfront, let alone adjust, especially when the degree of light regulation in the underlying photoreceptor is altogether limited. Against this backdrop, we deem it an advantage to now have at disposal a suite of several red-light-regulated PDEs with varying cellular activity and performance. By the same token, a recently characterized rhodopsin-based light-activated PDE from a flagellate expands and diversifies the optogenetic toolkit [43–45]. Compared to LAPD, this PDE is membrane-integral, is sensitive to other light colors, and primarily responds to illumination with changes in substrate affinity rather than maximal turnover.

cNMP-specific PDEs sensitive to red/far-red light are well suited for multiplexing with photoactivated nucleotidyl cyclases that mostly respond to light of shorter wavelengths [23,24,39–41]. The combination of individually addressable nucleotidyl cyclases and PDEs affords bimodal control by light of intracellular cyclic mononucleotides. Moreover, by optogenetically regulating both the making and breaking of cNMPs, a net regulatory effect much surpassing those of the light-regulated cyclase or PDE alone might be achieved [35]. This aspect is borne out in certain photoreceptors, which act as both histidine kinases and phosphatases and exhibit very stringent light responses [53]. Nucleotidyl cyclases and PDEs may also be paired with genetically encoded, fluorescent cNMP biosensors to enable all-optical experiments [60,61], in which acute cNMP levels inside cells are continuously read out to allow optogenetic feedback control of the light-sensitive actuators. As covered in the introduction, cyclic mononucleotides are integral to manifold physiological pathways, thus offering diverse toeholds for optogenetic intervention. As a case in point, the so-called two-component optogenetics strategy [62] combines photoreceptors, which generate primary responses, with secondary, light-inert components that latch onto these first responses and alter them in modality, time, space and amplitude. In a recent manifestation of this concept, a bacterial K^+-selective CNG channel was used in conjunction with a blue-light-sensitive PAC to trigger light-induced potassium currents and concomitant neuronal silencing [63]. Arguably, the sensitivity of the modular two-component approach may be extended to the red/far-red spectral region through combination with one of the BphP-PDE variants engineered presently. As of now, the *Dr*-*Bt*PDE2A variant appears best-suited for this approach.

Bacteriophytochrome engineering and signal transduction

Whereas three of the parallel design strategies pursued here eventually yielded novel light-activated PDEs, the exchange of the catalytic effector module clearly emerges as the simplest and at the same time, most successful strategy. Directly modeled on the LAPD template, the substitution of the effector unit for homologous modules readily yielded functional PDE variants, which in certain cases exhibited enhanced regulatory traits compared to LAPD. Arguably, this design strategy benefitted from high sequence homology among vertebrate PDE2A enzymes, including within the coiled-coil linker region (see Fig. 1d). Strikingly, the converse and equally obvious approach of replacing the entire PAS-GAF-PHY PCM of LAPD for the photosensors of other BphPs failed, despite pronounced, if somewhat lower, levels of sequence homology among the various PCMs. In marked contrast, the recent redesign of a red-light-sensitive PAC [28] via modular exchange of its *Dr*BphP unit, that it shares with LAPD, for PCMs from other BphPs proved straightforward [29]. Beyond effector identity, this design also differed in employing a somewhat more C-terminal junction site within the *Dr*BphP coiled-coil linker (see Fig. S4). Evidently, LAPD represents a local optimum in BphP-PDE design space, as most alterations, be they extensive (see Fig. 2b), be they small (see Fig. 3), are detrimental. These observations are surprising given that LAPD employs the *Dr*BphP PCM, yet its construction was based on the PCM structure of *Pa*BphP [36]; put another way, the original LAPD design does not stipulate the use of any particular BphP (other than *Pa*BphP), let alone of *Dr*BphP. Although a full molecular understanding is lacking, we concluded that the junction between the PCM and PDE modules, as configured in the original LAPD, is particularly conducive to signal transduction and should hence be preserved. In a first, rather coarse approach, we retained the *Dr*PHY domain thus leaving the junction intact, albeit at the cost of introducing a new seam between the GAF and PHY domains within the PCM. That notwithstanding, the strategy yielded light-activated PDEs, which, however, exhibited impaired photochemical properties (see Fig. 4). In a similar vein, by pursuing a more limited exchange of the PHY tongue region between PCMs, the regulatory response of an

engineered BphP has recently been greatly boosted [64], a rationale that may be transferrable to LAPD. In a second, more subtle approach, we altered the linker region of intact homologous PCMs near the junction site toward the GERL motif present in LAPD. Although not successful in all cases, most BphP-PDEs could be endowed with light responsiveness in this manner. Taken together, the above strategies pave the way toward the generation of additional BphP-PDEs, ideally with low dark activity, strong activation by red and/or far-red light, and full reversibility.

Given the above pitfalls and our ultimately incomplete molecular understanding, it is challenging to much extrapolate, let alone infer fail-safe design recipes. Nonetheless, several general aspects inform future efforts directed at engineering BphP photoreceptors. First, in combination with previous work [28,29,64,65], our study reveals that to a certain extent BphP photosensor modules (or constituent fragments) are mutually interchangeable. By extension, this observation implies shared, if not necessarily universal, signal-transduction mechanisms among and potentially even transcending BphPs. Second, additional molecular determinants, beyond the sheer (re)combination of protein domains, govern activity and regulation in composite (photo)receptors. Specifically, the inter-domain junctions mediate efficient communication between photosensor and effector entities. Although not probed here, previous work pinpointed the length of these, often α-helical, linkers as important parameters [27,28,36,53,54]; as we show presently, the sequence and specific molecular interactions of these linkers can be crucial factors as well. Third, effector identity determines the difficulty of a particular protein engineering task, and by extension, its ultimate success or failure. As a case in point, the derivatization of BphP-based PACs proved efficient [29] but that of BphP-PDEs, such as LAPD, did not, although some of the same BphP modules were used. Not only the sensor module but also the effector can profoundly affect receptor traits, as exemplified by the exchange of the PDE effector unit in LAPD (see Figs. 4 and 5). Specific receptor properties may not even be associated with a given photosensor or effector per se but rather a particular combination thereof. Hence, the characteristics of a receptor are often hard to exactly recapitulate a posteriori, and even harder to predict or plan a priori. Fourth, the engineering of actuators for optogenetics often strives to attain several desiderata in parallel, for example, optimization of diverse photochemical and catalytic aspects [35], which may be difficult to simultaneously realize in a single receptor variant, thus further complicating the design process. Against this backdrop, functional and genuinely light-regulated receptors, be they of natural origin, be they engineered, serve as valuable starting points for further, often iterative engineering efforts. The present and related previous studies [27–29,36,65] showcase a range of principal design strategies, which may be pursued to this end. That notwithstanding, the key to eventual success will likely often be the ability to construct and readily assess for light-regulated function many design variants in parallel.

Materials and Methods

Molecular biology

The LAPD gene, encoding the PCM of *D. radiodurans* BphP (Uniprot BPHY_DEIRA, residues 1–506) fused to the catalytic effector domain of *H. sapiens* PDE 2A (PDE2A_HUMAN, residues 555–941) and a C-terminal hexahistidine tag, was amplified by PCR from a previous pASK43 expression vector [36] and subcloned into a pCDFDuet plasmid (Novagen, Merck, Darmstadt, Germany) by Gibson assembly [66]. The gene encoding *Synechocystis* sp. heme oxygenase 1 (*Ss*HO) was PCR-amplified from plasmid pKT270 [51] and cloned by Gibson assembly into the pCDFDuet vector as well, such that within the resultant pCDF-LAPD-HO plasmid, expression of both LAPD and *Ss*HO is under control of T7-lacO promoters. Residue substitutions in LAPD were introduced by site-directed mutagenesis in the pCDF-LAPD-HO background. LAPD variants were generated by Gibson assembly in the same background via replacement of either the BphP PCM, the PDE unit, or both for homologous modules from BphPs and PDEs, respectively. Specifically, the PCM of *P. aeruginosa* BphP (BPHY_PSEAE, 1–497) was derived from a previous pET-24a vector [47]; genes for the BphP PCMs from *Azorhizobium caulinodans* (GenBank WP_012169446.1, 1–502), *Acaryochloris* sp. CCMEE 5410 (WP_010479127.1, 1–531), *A. tumefaciens* P1 (WP_010971984.1, 1–493), *A. tumefaciens* P2 (WP_004430460.1, 1–500), *Agrobacterium vitis* (WP_015916920.1, 1–499), *D. deserti* (WP_012695070.1, 1–520), *Hymenobacter swuensis* (AHJ98859.1, 1–515), *Idiomarina* sp. A28L (WP_007419415.1, 1–507), *Janthinobacterium* sp. CG23_2 (WP_054263721.1, 1–518), *Pleurocapsa* sp. PCC7319 (WP_019503487.1, 1–523), *Rhizobium etli* (WP_004673045.1, 1–502), *Rhizobium leguminosarum* (WP_077988302.1, 1–502), *R. palustris* P5 (WP_119019282.1, 1–500), *R. sphaeroides* (AMJ49789.1, 1–502), and *Xanthomonas campestris* (WP_011270102.1, 1–512) were synthesized with *E. coli*-adapted codon usage (GeneArt, Regensburg, Germany). The PCM of *P. syringae* BphP (RMN66899.1, 1–626) was obtained by PCR amplification from genomic DNA. In case of the effector module, genes with *E. coli*-adapted codon

usage were synthesized for the PDE2A homologs from *Alligator mississippiensis* (KYO25631.1, 538–925), *B. taurus* (XP_024830786.1, 636–1022), *P. cinereus* (XP_020845306.1, 566–953), *Rattus norvegicus* (NP_112341.1, 543–928), and *X. tropicalis* (NP_001072607.1, 558–951). For the PAS-GAF exchange variants, the N-terminal part of LAPD (residues 1–323) was replaced by corresponding parts from homologous BphPs as follows: *P. aeruginosa* (1–310), *A. caulinodans* (1–312), *Acaryochloris* sp. CCMEE 5410 (1–339), *A. tumefaciens* P1 (1–304), *A. tumefaciens* P2 (1–311), *D. deserti* (1–321), *Janthinobacterium* sp. CG23_2 (1–320), *P. syringae* (1–324), *R. sphaeroides* (1–362), and *X. campestris* (1–321). For expression in eukaryotic cells, select LAPD variants were subcloned into the pCDNA3.1+ vector (Invitrogen, ThermoFisher Scientific) with C-terminal mCherry and HA tags. To facilitate eukaryotic expression, genes for *D. radiodurans* and *D. deserti* BphP, as well as *H. sapiens* and *B. taurus* PDE2A with human-adapted codon usage were synthesized and used in place of the genes with bacterial codon adaptation. The identity of all constructs was confirmed by Sanger DNA sequencing (GATC, Konstanz, Germany; or, Microsynth Seqlab, Göttingen, Germany).

Protein expression and purification

pCDFDuet plasmids encoding individual PDE variants and *Ss*HO were transformed into BL21 (DE3) or LOBSTR BL21(DE3) cells [67]. Resultant transformants were used to inoculate two baffled flasks with 800 mL lysogeny broth (LB) medium supplemented with 100 µg mL^{-1} streptomycin (Strep). Bacterial cultures were grown at 37 °C and 225 rpm until an optical density at 600 nm (OD_{600}) of around 0.6 was reached, at which point the temperature was lowered to 16 °C and 0.5 mM δ-amino levulinic acid (δ-ALA) was added. Expression of the PDE variant and *Ss*HO was induced by addition of 1 mM isopropyl β-D-1-thiogalactopyranoside (IPTG), and cultivation continued at 16 °C and 225 rpm for 16 h. Purification of LAPD variants was conducted similar to previous protocols [36]. Briefly, cells were harvested by centrifugation, resuspended in buffer [50 mM Tris/HCl (pH 8.0), 20 mM NaCl, 20 mM imidazole] and supplemented with protease inhibitors (cOmplete Ultra, Roche Diagnostics, Mannheim, Germany). After lysis by ultrasound or microfluidizer and centrifugation, the supernatant was incubated for 1 h at 4 °C with 100 µM biliverdin hydrochloride (Livchem Logistics GmbH, Frankfurt, Germany) and 5 mM Tris-(2-carboxyethyl)-phosphine. The lysate was then applied to Co^{2+}- or Ni^{2+}-nitrilotriacetic acid affinity resin (HisPur Cobalt Resin, ThermoFisher Scientific, Dreieich, Germany, or, Protino Ni-NTA, Macherey & Nagel GmbH, Düren, Germany). Following washing and elution with 200 mM imidazole, the protein was dialyzed into buffer [50 mM Tris/HCl (pH 8.0, 20 mM NaCl] and purified by anion-exchange chromatography (HiTrap Q HP, GE Healthcare, Munich, Germany). Purity was analyzed by denaturing polyacrylamide gel electrophoresis (PAGE) and Coomassie staining; covalent chromophore incorporation was assessed by Zn^{2+}-induced bilin fluorescence [52]. Fractions containing pure protein were pooled, dialyzed into storage buffer [50 mM Tris/HCl (pH 8.0), 20 mM NaCl, 20% (w/v) glycerol] and concentrated by spin filtration (Vivaspin 6, 10-kDa cutoff, GE Healthcare). Sample concentration was determined by absorption measurements (8453 UV–vis, Agilent Technologies, Waldbronn, Germany) using a molar extinction coefficient of 45,700 M^{-1} cm^{-1} at the isosbestic point (724 nm) [68]. For storage, protein aliquots were flash-frozen in liquid nitrogen and stored at −80 °C.

Western blot analysis of bacterial expression

To verify bacterial expression of the BphP-PDE variants, bacterial clones harboring pCDFDuet expression plasmids (see above) were grown in 5 mL LB/Strep liquid culture in darkness at 37 °C until an OD_{600} between 0.6 and 0.8 was reached. PDE expression was induced by addition of 1 mM IPTG and 0.5 mM δ-ALA, the temperature lowered to 16 °C, and incubation continued for 20 h. To verify protein expression, the bacterial cells were pelleted by centrifugation and resuspended in 500 µL Laemmli loading buffer [62.5 mM Tris/HCl (pH 6.8), 2.5% (w/v) SDS, 0.002% (w/v) bromophenol blue, 5% (v/v) 2-mercaptoethanol, 10% (w/v) glycerol]. Samples were denatured at 95 °C, cleared by centrifugation and separated via denaturing PAGE. The resulting gels were transferred onto a PVDF membrane by semi-dry blotting (Bio-Rad Laboratories GmbH, München, Germany). The membrane was washed with TBS-Tween buffer [20 mM Tris/HCl (pH 7.5), 150 mM NaCl, 0.1% (v/v) Tween 20] and blocked with TBS-Tween plus 3% (w/v) bovine serum albumin (BSA), followed by incubation at 4 °C over night with the primary mouse anti-His antibody (MA1-21315 Pierce 5x-His Epitope Tag Antibody His.H8, ThermoFisher Scientific) in TBS-Tween/BSA. After extensive washing with TBS-Tween, the secondary anti-mouse antibody (A3562 anti-mouse IgG-alkaline phosphatase; Sigma-Aldrich) was added for 4 h at 22 °C. After renewed washing with TBS-Tween, the membranes were incubated in development buffer for 2 min at 22 °C [100 mM/Tris–HCl (pH 9.5), 100 mM NaCl, 5 mM $MgCl_2$, 30 µg L^{-1} nitroblue tetrazolium, 15 µg L^{-1} 5-bromo-4-chloro-3-indolyl phosphate]. The reaction was stopped by rinsing the membranes thoroughly with water, and the membranes were dried and photographed with a digital camera.

PDE activity measurements

For the determination of PDE activity in crude lysate [49], bacterial clones harboring pCDFDuet expression plasmids were grown in 5-mL scale as described above. After induction and overnight expression at 16 °C, 2 mL of each culture were centrifuged, the supernatant discarded, and the pellet resuspended in buffer AB I [2 mM potassium phosphate (pH 7.6), 5 mM $MgCl_2$, 100 mM KCl, 10 mM dithiothreitol, 0.04% (w/v) bovine serum albumin]. Lysis was accomplished by three cycles of freezing in liquid nitrogen and thawing. Lysate (10 µL) was transferred to a clear 96-well microtiter plate (MTP) and 60 µL buffer AB II [0.5 µM 2′,7′-bis-(2-carboxyethyl)-(5-and-6)-carboxyfluorescein (BCECF [50], ThermoFisher Scientific) in buffer AB I] were added. Following equilibration at 29 °C in darkness, the samples were either kept in darkness or illuminated with red light [(670 ± 15) nm, 500 µW cm^{-2}, 10 s] or far-red light [(780 ± 15) nm, 500 µW cm^{-2}, 10 s]. The PDE reaction was initiated via addition of 2 mM cGMP (Sigma-Aldrich, Darmstadt, Germany). Using a CLARIOstar multimode MTP reader (BMG Labtech GmbH, Ortenberg, Germany), BCECF fluorescence intensities F_{440} and F_{500} were measured over time at excitation wavelengths of (440 ± 5) and (500 ± 5) nm, respectively, and a joint emission wavelength of (560 ± 30) nm. The ratio of F_{500} over F_{440} was corrected for buffer background and plotted as a function of time. The early time course was fitted to a linear function to determine initial reaction velocities. All measurements were performed in biological triplicates. Unless stated otherwise, data were evaluated and plotted with the Fit-o-mat program [69].

The catalytic activity of purified PDE variants was addressed by high-performance liquid chromatography (HPLC). Enzyme (20 nM) was incubated at 29 °C or 37 °C in 700 µL reaction buffer [20 mM Tris/HCl (pH 8.0), 20 mM NaCl] in darkness, under red light [(670 ± 15) nm, 80 µW cm^{-2}, 60 s], or under red light followed by far-red light [(780 ± 15) nm, 80 µW cm^{-2}, 60 s]. Reactions were started by addition of 1 mM substrate cGMP or cAMP (Merck), and 50 µL aliquots were drawn at discrete timepoints and rapidly inactivated by incubation at 95 °C for 1 min. Samples were cleared by centrifugation for 5 min at 20,000*g* and filtered (Chromafil, 0.2-µm pore size, Macherey & Nagel GmbH), followed by HPLC analysis on reversed-phase (RP) C18 columns using isocratic elution with 97% (v/v) 100 mM potassium phosphate pH 5.5 and 3% (v/v) acetonitrile. In case of cGMP, the samples were analyzed on a Eurospher II C18 RP column (Knauer, Berlin, Germany) using a Smartline HPLC system (Knauer). cAMP hydrolysis reactions were assessed on a Kinetex 5 µ EVO C18 RP column (Phenomenex, Torrance, USA) and an Acquity UPLC (Waters GmbH, Eschborn, Germany). Peak areas for the cGMP and cAMP hydrolysis reactions were integrated with the OpenLAB (Agilent) or Empower (Waters) programs and calibrated against cAMP, cGMP, AMP, and GMP standards. All measurements were performed in triplicate.

Eukaryotic cell culture

Cell culture experiments were conducted with HEK-TM cells, derived from HEK293 ATCC cells, which stably express a variant of the cyclic nucleotide-gated ion channel CNGA2 [59]. Cells were incubated at 37 °C and 5% (v/v) CO_2 (HERAcell 240, ThermoFisher Scientific). DMEM medium was obtained from Gibco (ThermoFisher Scientific) and supplemented with 10% (v/v) fetal calf serum (Biochrom, Berlin, Germany) and 100 µg mL^{-1} hygromycin. The HEK-TM cell line stably expressing LAPD was maintained in medium containing 50 µg mL^{-1} hygromycin and 5 µg mL^{-1} blasticidin (Invitrogen). Cells were transfected using Lipofectamine 2000 (Life Technologies, Carlsbad, USA) according to the manufacturer's protocol. Stable HEK-TM cell lines were established for the LAPD variants *Dr-Bt*PDE, *Dr-Pc*PDE and *Dr-Xt*PDE and maintained in medium containing 100 µg mL^{-1} hygromycin and 0.8 mg mL^{-1} G418 (Geneticin, Gibco, ThermoFisher Scientific).

Western blot analysis and immunocytochemistry

The expression of the PDE variants in HEK-TM cells was ascertained by immunochemical approaches. For Western blot analysis, HEK-TM cells were lysed [10 mM Tris/HCl (pH 7.6), 140 mM NaCl, 1 mM EDTA, 1.0% (v/v) Triton-X 100, protease inhibitor cocktail (Sigma-Aldrich, no. P8340)] on ice for 30 min, followed by centrifugation (10 min, 10,000 *g*, 4 °C). The protein concentration of the supernatant was determined in a bicinchoninic acid assay, and samples were analyzed by denaturing PAGE followed by semi-dry blotting (Carl Roth, Karlsruhe, Germany) on a PVDF membrane (Immobilon-FL, Merck). The blots were stained using primary antibodies against mCherry (0.22 µg mL^{-1}, rabbit polyclonal, Rockland Immunochemicals Inc., Limerick, USA, no. 600-401-379); β tubulin (31.3 µg mL^{-1}, mouse monoclonal, Sigma, no. T4026); and the CNGA2 channel (3B10, [70]). The following secondary antibodies were used: donkey anti-rabbit IRDye680LT (LI-COR Biosciences, Bad Homburg, Germany, no. 925-68023); donkey anti-mouse IRDye680LT (LI-COR Biosciences, no. 926–68022); and donkey anti-mouse IRDye800CW (LI-COR Biosciences, no. 926-32212). Fluorescence was detected with an Odyssey imaging system (LI-COR Biosciences).

For immunocytochemical analysis, 10^5 cells each were seeded into wells containing a poly-L-lysine (PLL)-coated 13-mm coverslip. After one day incubation, the cells were washed with PBS [10 mM Na_2HPO_4,

1.8 mM KH_2PO_4, 137 mM NaCl, 2.7 mM KCl (pH 7.4)] and fixed in 4% (v/v) paraformaldehyde. After washing with PBS, the cells were blocked by addition of 300 µL blocking buffer [5% (v/v) ChemieBlocker (Millipore, Merck), 0.5% (v/v) Triton-X 100, in PBS] for 30 min. Cells were then incubated for 60 min with anti-mCherry primary antibody (1.83 µg ml^{-1}) in blocking buffer. After washing with PBS, 150 µL blocking buffer containing fluorescently labeled secondary antibody [4 µg mL^{-1}, goat anti-rabbit Alexa Fluor 488 (AF488), Life Technologies, no. A-11034] and 0.5 mg mL^{-1} 2-(4-amidinophenyl)-1H-indole-6-carboxamidine (DAPI, ThermoFisher Scientific) were added. Following incubation for 60 min in darkness and washing, the coverslips were mounted in Aqua-Poly/Mount (Polysciences, Warrington, USA). The slides were then analyzed on a fluorescence microscope (Eclipse Ti, Nikon) using excitation and emission wavelengths of 408/417–477 nm for DAPI, 561/570–1000 nm for mCherry and 488/500–550 nm for AF488.

Phosphodiesterase activity measurements in HEK-TM cells

For PDE activity assays in eukaryotic cells, stable cell lines were seeded on a PLL-coated 96-well MTP at 3 × 10^4 cells per well and incubated over night at 37 °C and 5% (v/v) CO_2 in darkness. All following steps were conducted under dim green light. Medium was removed, and cells were washed with 50 µL ES buffer [120 mM NaCl, 5 mM KCl, 2 mM $CaCl_2$, 2 mM $MgCl_2$, 10 mM glucose, 10 mM HEPES (pH 7.4)]. Cells were loaded with 2 µM Fluo4-AM and 3 mM probenecid in 50 µL ES buffer and incubated for 30 min at 29 or 37 °C. Afterward, the buffer was replaced with 90 µL ES containing 3 mM probenecid, and the MTP was incubated at 29 or 37 °C for 30 min inside a multimode MTP reader (FLUOstar omega, BMG Labtech). Fluorescence was measured with excitation and emission wavelengths of (485 ± 6) and (530 ± 15) nm, respectively, and the gain was adjusted for the stable LAPD cell line. After 2 min, 100 µM NKH477 (Sigma-Aldrich) in ES buffer was added, and measurements continued for 15 min. In controls, ES buffer was added rather than the NKH477 solution. During the measurement, the plate was first illuminated with an 850-nm LED mounted inside the MTP reader. At a set point, the illumination switched to a 690-nm LED for activation of the LAPD variants. After an additional 6 min, 2 µM ionomycin was added, and fluorescence was recorded until a maximal response was observed. For the transiently transfected HEK-TM cells (see Fig. S9b), the experiment was conducted at 29 °C and the timing of the illumination was different, but other than that, the experiments were conducted in the same manner.

Supplementary data to this article can be found online at https://doi.org/10.1016/j.jmb.2019.07.011.

Acknowledgments

We thank past and present members of the Möglich and Wachten laboratories for support and comments, and Thessa Jacob for assistance with HPLC analysis. Funding through the Deutsche Forschungsgemeinschaft (grant MO2192/4-1 to A. M.; SPP1926 grant WA3382/2-1, SPP1726 grant WA3382/3-1, and under Germany's Excellence Strategy: EXC2151-390873048 to D.W.), the Alexander von Humboldt Foundation (Sofja-Kovalevskaya Award to A.M.), and the Boehringer Ingelheim Fonds (to J.N.H.) is gratefully appreciated.

Declaration of Competing Interest

None.

Received 26 February 2019;
Received in revised form 22 June 2019;
Accepted 2 July 2019
Available online 10 July 2019

Keywords:
bacteriophytochrome;
cyclic mononucleotide;
optogenetics;
phosphodiesterase;
sensory photoreceptor

Abbreviations used:
cAMP and cGMP, 3′, 5′-cyclic adenosine and guanosine monophosphate; CNG, cyclic nucleotide-gated; cNMP, cyclic nucleoside monophosphate; PDE, phosphodiesterase; PAC, photoactivated adenylyl cyclase; PCM, photosensory core module; BphP, bacterial phytochrome.

References

[1] Gerhard. Krauss, Biochemistry of Signal Transduction and Regulation., Wiley-VCH, 2014.
[2] T.W. Rall, E.W. Sutherland, Formation of a cyclic adenine ribonucleotide by tissue particles, J. Biol. Chem. 232 (1958) 1065–1076.

[3] D.F. Ashman, R. Lipton, M.M. Melicow, T.D. Price, Isolation of adenosine 3′, 5′-monophosphate and guanosine 3′, 5′-monophosphate from rat urine, Biochem. Biophys. Res. Commun. 11 (1963) 330–334.
[4] T.W. Rall, E.W. Sutherland, J. Berthet, The relationship of epinephrine and glucagon to liver phosphorylase. IV. Effect of epinephrine and glucagon on the reactivation of phosphorylase in liver homogenates, J. Biol. Chem 224 (1957) 463–475.
[5] J.F. Kuo, P. Greengard, Cyclic nucleotide-dependent protein kinases. VI. Isolation and partial purification of a protein kinase activated by guanosine 3′,5′-monophosphate, J. Biol. Chem. 245 (1970) 2493–2498.
[6] D.A. Walsh, J.P. Perkins, E.G. Krebs, An adenosine 3′,5'-monophosphate-dependent protein kinase from rabbit skeletal muscle, J. Biol. Chem. 243 (1968) 3763–3765.
[7] E.E. Fesenko, S.S. Kolesnikov, A.L. Lyubarsky, Induction by cyclic GMP of cationic conductance in plasma membrane of retinal rod outer segment, Nature. 313 (1985) 310–313, https://doi.org/10.1038/313310a0.
[8] J. de Rooij, F.J.T. Zwartkruis, M.H.G. Verheijen, R.H. Cool, S.M.B. Nijman, A. Wittinghofer, J.L. Bos, Epac is a Rap1 guanine-nucleotide-exchange factor directly activated by cyclic AMP, Nature. 396 (1998) 474–477, https://doi.org/10.1038/24884.
[9] B. Andrée, T. Hillemann, G. Kessler-Icekson, T. Schmitt-John, H. Jockusch, H.-H. Arnold, T. Brand, Isolation and characterization of the novel Popeye gene family expressed in skeletal muscle and heart, Dev. Biol. 223 (2000) 371–382, https://doi.org/10.1006/dbio.2000.9751.
[10] J.N. Marden, Q. Dong, S. Roychowdhury, J.E. Berleman, C. E. Bauer, Cyclic GMP controls Rhodospirillum centenum cyst development, Mol. Microbiol. 79 (2011) 600–615, https://doi.org/10.1111/j.1365-2958.2010.07513.x.
[11] M. Gomelsky, cAMP, c-di-GMP, c-di-AMP and now cGMP: bacteria use them all! Mol. Microbiol. 79 (2011) 562–565, https://doi.org/10.1111/j.1365-2958.2010.07514.x.
[12] T. Shimada, N. Fujita, K. Yamamoto, A. Ishihama, Novel roles of cAMP receptor protein (CRP) in regulation of transport and metabolism of carbon sources, PLoS One 6 (2011), e20081. https://doi.org/10.1371/journal.pone.0020081.
[13] B. Görke, J. Stülke, Carbon catabolite repression in bacteria: many ways to make the most out of nutrients, Nat. Rev. Microbiol. 6 (2008) 613–624, https://doi.org/10.1038/nrmicro1932.
[15] M. Conti, J. Beavo, Biochemistry and physiology of cyclic nucleotide phosphodiesterases: essential components in cyclic nucleotide signaling, Annu. Rev. Biochem. 76 (2007) 481–511, https://doi.org/10.1146/annurev.biochem.76.060305.150444.
[16] S.H. Francis, M.A. Blount, J.D. Corbin, Mammalian cyclic nucleotide phosphodiesterases: molecular mechanisms and physiological functions, Physiol. Rev. 91 (2011) 651–690, https://doi.org/10.1152/physrev.00030.2010.
[17] J. Pandit, M.D. Forman, K.F. Fennell, K.S. Dillman, F.S. Menniti, Mechanism for the allosteric regulation of phosphodiesterase 2A deduced from the x-ray structure of a near full-length construct, Proc. Natl. Acad. Sci. U. S. A. 106 (2009) 18225–18230, https://doi.org/10.1073/pnas.0907635106.
[18] K. Deisseroth, G. Feng, A.K. Majewska, G. Miesenböck, A. Ting, M.J. Schnitzer, Next-generation optical technologies for illuminating genetically targeted brain circuits, J. Neurosci. 26 (2006) 10380–10386, https://doi.org/10.1523/JNEUROSCI.3863-06.2006.
[19] V. Jansen, J.F. Jikeli, D. Wachten, How to control cyclic nucleotide signaling by light, Curr. Opin. Biotechnol. 48 (2017) 15–20, https://doi.org/10.1016/j.copbio.2017.02.014.
[20] A. Losi, K.H. Gardner, A. Möglich, Blue-light receptors for optogenetics, Chem. Rev. 118 (2018) 10659–10709, https://doi.org/10.1021/acs.chemrev.8b00163.
[21] M. Iseki, S. Matsunaga, A. Murakami, K. Ohno, K. Shiga, K. Yoshida, M. Sugai, T. Takahashi, T. Hori, M. Watanabe, A blue-light-activated adenylyl cyclase mediates photoavoidance in *Euglena gracilis*, Nature. 415 (2002) 1047–1051, https://doi.org/10.1038/4151047a.
[22] S. Schröder-Lang, M. Schwärzel, R. Seifert, T. Strünker, S. Kateriya, J. Looser, M. Watanabe, U.B. Kaupp, P. Hegemann, G. Nagel, Fast manipulation of cellular cAMP level by light in vivo, Nat. Methods 4 (2007) 39–42, https://doi.org/10.1038/nmeth975.
[23] M. Stierl, P. Stumpf, D. Udwari, R. Gueta, R. Hagedorn, A. Losi, W. Gärtner, L. Petereit, M. Efetova, M. Schwarzel, T.G. Oertner, G. Nagel, P. Hegemann, Light-modulation of cellular cAMP by a small bacterial photoactivated adenylyl cyclase, bPAC, of the soil bacterium beggiatoa, J. Biol. Chem. 286 (2011) 1181–1188, https://doi.org/10.1074/jbc.M110.185496.
[24] M.-H. Ryu, O.V. Moskvin, J. Siltberg-Liberles, M. Gomelsky, Natural and engineered photoactivated nucleotidyl cyclases for optogenetic applications, J. Biol. Chem. 285 (2010) 41501–41508, https://doi.org/10.1074/jbc.M110.177600.
[25] S. Raffelberg, L. Wang, S. Gao, A. Losi, W. Gärtner, G. Nagel, A LOV-domain-mediated blue-light-activated adenylate (adenylyl) cyclase from the cyanobacterium *Microcoleus chthonoplastes* PCC 7420, Biochem. J. 455 (2013) 359–365, https://doi.org/10.1042/BJ20130637.
[26] M. Blain-Hartung, N.C. Rockwell, M.V. Moreno, S.S. Martin, F. Gan, D.A. Bryant, J.C. Lagarias, Cyanobacteriochrome-based photoswitchable adenylyl cyclases (cPACs) for broad spectrum light regulation of cAMP levels in cells, J. Biol. Chem. 293 (2018) 8473–8483, https://doi.org/10.1074/jbc.RA118.002258.
[27] M.-H. Ryu, I.-H. Kang, M.D. Nelson, T.M. Jensen, A.I. Lyuksyutova, J. Siltberg-Liberles, D.M. Raizen, M. Gomelsky, Engineering adenylate cyclases regulated by near-infrared window light, Proc. Natl. Acad. Sci. U. S. A. 111 (2014) 10167–10172, https://doi.org/10.1073/pnas.1324301111.
[28] S. Etzl, R. Lindner, M.D. Nelson, A. Winkler, Structure-guided design and functional characterization of an artificial red light-regulated guanylate/adenylate cyclase for optogenetic applications, J. Biol. Chem. 293 (2018) 9078–9089, https://doi.org/10.1074/jbc.RA118.003069.
[29] B. Stüven, R. Stabel, R. Ohlendorf, J. Beck, R. Schubert, A. Möglich, Characterization and engineering of photoactivated adenylyl cyclases, Biol. Chem. 400 (2019) 429–441, https://doi.org/10.1515/hsz-2018-0375.
[30] G. Gourinchas, S. Etzl, A. Winkler, Bacteriophytochromes — from informative model systems of phytochrome function to powerful tools in cell biology, Curr. Opin. Struct. Biol. 57 (2019) 72–83, https://doi.org/10.1016/j.sbi.2019.02.005.
[31] N.C. Rockwell, J.C. Lagarias, A brief history of phytochromes, Chemphyschem. 11 (2010) 1172–1180, https://doi.org/10.1002/cphc.200900894.
[32] H. Takala, A. Björling, O. Berntsson, H. Lehtivuori, S. Niebling, M. Hoernke, I. Kosheleva, R. Henning, A. Menzel, J.A. Ihalainen, S. Westenhoff, Signal amplification and

transduction in phytochrome photosensors, Nature. 509 (2014) 245–248, https://doi.org/10.1038/nature13310.
[33] E.S. Burgie, J. Zhang, R.D. Vierstra, Crystal structure of deinococcus phytochrome in the photoactivated state reveals a cascade of structural rearrangements during photoconversion, Structure. 24 (2016) 448–457, https://doi.org/10.1016/j.str.2016.01.001.
[34] R. Weissleder, A clearer vision for *in vivo* imaging, Nat. Biotechnol. 19 (2001) 316–317, https://doi.org/10.1038/86684.
[35] T. Ziegler, A. Möglich, Photoreceptor engineering, Front. Mol. Biosci. 2 (2015) 30, https://doi.org/10.3389/fmolb.2015.00030.
[36] C. Gasser, S. Taiber, C.-M. Yeh, C.H. Wittig, P. Hegemann, S. Ryu, F. Wunder, A. Möglich, Engineering of a red-light-activated human cAMP/cGMP-specific phosphodiesterase, Proc. Natl. Acad. Sci. U. S. A. 111 (2014) 8803–8808, https://doi.org/10.1073/pnas.1321600111.
[37] G.S. Filonov, K.D. Piatkevich, L.-M. Ting, J. Zhang, K. Kim, V. V. Verkhusha, Bright and stable near-infrared fluorescent protein for in vivo imaging, Nat. Biotechnol. 29 (2011) 757–761, https://doi.org/10.1038/nbt.1918.
[38] T. Kim, M. Folcher, M.D.-E. Baba, M. Fussenegger, A synthetic erectile optogenetic stimulator enabling blue-light-inducible penile erection, Angew. Chem. Int. Ed. 54 (2015) 5933–5938, https://doi.org/10.1002/anie.201412204.
[39] G.M. Avelar, R.I. Schumacher, P.A. Zaini, G. Leonard, T.A. Richards, S.L. Gomes, A rhodopsin-guanylyl cyclase gene fusion functions in visual perception in a fungus, Curr. Biol. 24 (2014) 1234–1240, https://doi.org/10.1016/j.cub.2014.04.009.
[40] U. Scheib, K. Stehfest, C.E. Gee, H.G. Körschen, R. Fudim, T.G. Oertner, P. Hegemann, The rhodopsin–guanylyl cyclase of the aquatic fungus Blastocladiella emersonii enables fast optical control of cGMP signaling, Sci. Signal. 8 (2015) rs8-rs8, https://doi.org/10.1126/scisignal.aab0611.
[41] S. Gao, J. Nagpal, M.W. Schneider, V. Kozjak-Pavlovic, G. Nagel, A. Gottschalk, Optogenetic manipulation of cGMP in cells and animals by the tightly light-regulated guanylyl-cyclase opsin CyclOp, Nat. Commun. 6 (2015) 8046, https://doi.org/10.1038/ncomms9046.
[42] Y. Tian, S. Gao, E.L. von der Heyde, A. Hallmann, G. Nagel, Two-component cyclase opsins of green algae are ATP-dependent and light-inhibited guanylyl cyclases, BMC Biol. 16 (2018) 144, https://doi.org/10.1186/s12915-018-0613-5.
[43] K. Yoshida, S.P. Tsunoda, L.S. Brown, H. Kandori, A unique choanoflagellate enzyme rhodopsin exhibits light-dependent cyclic nucleotide phosphodiesterase activity, J. Biol. Chem. 292 (2017) 7531–7541, https://doi.org/10.1074/jbc.M117.775569.
[44] L.B. Lamarche, R.P. Kumar, M.M. Trieu, E.L. Devine, L.E. Cohen-Abeles, D.L. Theobald, D.D. Oprian, Purification and characterization of RhoPDE, a retinylidene/phosphodiesterase fusion protein and potential optogenetic tool from the choanoflagellate *Salpingoeca rosetta*, Biochemistry. 56 (2017) 5812–5822, https://doi.org/10.1021/acs.biochem.7b00519.
[45] Y. Tian, S. Gao, S. Yang, G. Nagel, A novel rhodopsin phosphodiesterase from *Salpingoeca rosetta* shows light-enhanced substrate affinity, Biochem. J. 475 (2018) 1121–1128, https://doi.org/10.1042/BCJ20180010.
[46] V. Jansen, L. Alvarez, M. Balbach, T. Strünker, P. Hegemann, U.B. Kaupp, D. Wachten, Controlling fertilization and cAMP signaling in sperm by optogenetics, ELife. 4 (2015)https://doi.org/10.7554/eLife.05161.
[47] X. Yang, J. Kuk, K. Moffat, Crystal structure of *Pseudomonas aeruginosa* bacteriophytochrome: photoconversion and signal transduction, Proc. Natl. Acad Sci. U A. 105 (2008) 14715–14720.
[48] G. Rottwinkel, I. Oberpichler, T. Lamparter, Bathy phytochromes in rhizobial soil bacteria, J. Bacteriol. 192 (2010) 5124–5133, https://doi.org/10.1128/JB.00672-10.
[49] C.H. Schumacher, H.G. Körschen, C. Nicol, C. Gasser, R. Seifert, M. Schwärzel, A. Möglich, A fluorometric activity assay for light-regulated cyclic-nucleotide-monophosphate actuators, Methods Mol. Biol. Clifton NJ. 1408 (2016) 93–105, https://doi.org/10.1007/978-1-4939-3512-3_7.
[50] T.J. Rink, R.Y. Tsien, T. Pozzan, Cytoplasmic pH and free Mg^{2+} in lymphocytes, J. Cell Biol. 95 (1982) 189–196.
[51] K. Mukougawa, H. Kanamoto, T. Kobayashi, A. Yokota, T. Kohchi, Metabolic engineering to produce phytochromes with phytochromobilin, phycocyanobilin, or phycoerythrobilin chromophore in *Escherichia coli*, FEBS Lett. 580 (2006) 1333–1338, https://doi.org/10.1016/j.febslet.2006.01.051.
[52] T.R. Berkelman, J.C. Lagarias, Visualization of bilin-linked peptides and proteins in polyacrylamide gels, Anal. Biochem. 156 (1986) 194–201.
[53] A. Möglich, R.A. Ayers, K. Moffat, Design and signaling mechanism of light-regulated histidine kinases, J. Mol. Biol. 385 (2009) 1433–1444, https://doi.org/10.1016/j.jmb.2008.12.017.
[54] R. Ohlendorf, C.H. Schumacher, F. Richter, A. Möglich, Library-aided probing of linker determinants in hybrid photoreceptors, ACS Synth. Biol. 5 (2016) 1117–1126, https://doi.org/10.1021/acssynbio.6b00028.
[56] G. Gourinchas, S. Etzl, C. Göbl, U. Vide, T. Madl, A. Winkler, Long-range allosteric signaling in red light-regulated diguanylyl cyclases, Sci. Adv. 3 (2017), e1602498. https://doi.org/10.1126/sciadv.1602498.
[57] D. Bellini, M.Z. Papiz, Structure of a bacteriophytochrome and light-stimulated protomer swapping with a gene repressor, Structure. 20 (2012) 1436–1446, https://doi.org/10.1016/j.str.2012.06.002.
[58] L.H. Otero, S. Klinke, J. Rinaldi, F. Velázquez-Escobar, M.A. Mroginski, M. Fernández López, F. Malamud, A.A. Vojnov, P. Hildebrandt, F.A. Goldbaum, H.R. Bonomi, Structure of the full-length bacteriophytochrome from the plant pathogen *Xanthomonas campestris* provides clues to its long-range signaling mechanism, J. Mol. Biol. 428 (2016) 3702–3720, https://doi.org/10.1016/j.jmb.2016.04.012.
[59] S. Wachten, J. Schlenstedt, R. Gauss, A. Baumann, Molecular identification and functional characterization of an adenylyl cyclase from the honeybee, J. Neurochem. 96 (2006) 1580–1590, https://doi.org/10.1111/j.1471-4159.2006.03666.x.
[60] J.A. Kaczmarski, J.A. Mitchell, M.A. Spence, V. Vongsouthi, C.J. Jackson, Structural and evolutionary approaches to the design and optimization of fluorescence-based small molecule biosensors, Curr. Opin. Struct. Biol. 57 (2019) 31–38, https://doi.org/10.1016/j.sbi.2019.01.013.
[61] S. Mukherjee, V. Jansen, J.F. Jikeli, H. Hamzeh, L. Alvarez, M. Dombrowski, M. Balbach, T. Strünker, R. Seifert, U.B. Kaupp, D. Wachten, A novel biosensor to study cAMP dynamics in cilia and flagella, ELife. 5 (2016), e14052. https://doi.org/10.7554/eLife.14052.
[62] E.A. Ferenczi, J. Vierock, K. Atsuta-Tsunoda, S.P. Tsunoda, C. Ramakrishnan, C. Gorini, K. Thompson, S.Y. Lee, A. Berndt, C. Perry, S. Minniberger, A. Vogt, J. Mattis, R. Prakash, S. Delp, K. Deisseroth, P. Hegemann, Optogenetic

approaches addressing extracellular modulation of neural excitability, Sci. Rep. 6 (2016) 23947, https://doi.org/10.1038/srep23947.

[63] Y.A.B. Sierra, B.R. Rost, M. Pofahl, A.M. Fernandes, R.A. Kopton, S. Moser, D. Holtkamp, N. Masala, P. Beed, J.J. Tukker, S. Oldani, W. Bönigk, P. Kohl, H. Baier, F. Schneider-Warme, P. Hegemann, H. Beck, R. Seifert, D. Schmitz, Potassium channel-based optogenetic silencing, Nat. Commun. 9 (2018) 4611, https://doi.org/10.1038/s41467-018-07038-8.

[64] G. Gourinchas, U. Vide, A. Winkler, Influence of the N-terminal segment and the PHY-tongue element on light-regulation in bacteriophytochromes, J. Biol. Chem. 294 (2019) 4498–4510, https://doi.org/10.1074/jbc.RA118.007260.

[65] M.-H. Ryu, M. Gomelsky, Near-infrared light responsive synthetic c-di-GMP module for optogenetic applications, ACS Synth. Biol. 3 (2014) 802–810, https://doi.org/10.1021/sb400182x.

[66] D.G. Gibson, L. Young, R.-Y. Chuang, J.C. Venter, C.A. Hutchison, H.O. Smith, Enzymatic assembly of DNA molecules up to several hundred kilobases, Nat. Methods 6 (2009) 343–345, https://doi.org/10.1038/nmeth.1318.

[67] K.R. Andersen, N.C. Leksa, T.U. Schwartz, Optimized *E. coli* expression strain LOBSTR eliminates common contaminants from His-tag purification, Proteins Struct. Funct. Bioinforma. 81 (2013) 1857–1861. doi:https://doi.org/10.1002/prot.24364.

[68] J.R. Wagner, J. Zhang, D. von Stetten, M. Günther, D.H. Murgida, M.A. Mroginski, J.M. Walker, K.T. Forest, P. Hildebrandt, R.D. Vierstra, Mutational analysis of *Deinococcus radiodurans* bacteriophytochrome reveals key amino acids necessary for the photochromicity and proton exchange cycle of phytochromes, J. Biol. Chem. 283 (2008) 12212–12226.

[69] A. Möglich, An open-source, cross-platform resource for nonlinear least-squares curve fitting, J. Chem. Educ. 95 (2018) 2273–2278, https://doi.org/10.1021/acs.jchemed.8b00649.

[70] M.R. Meyer, A. Angele, E. Kremmer, U.B. Kaupp, F. Müller, A cGMP-signaling pathway in a subset of olfactory sensory neurons, Proc. Natl. Acad. Sci. 97 (2000) 10595–10600, https://doi.org/10.1073/pnas.97.19.10595.